Priority Report

Cancer Research

PARPi Triggers the STING-Dependent Immune Response and Enhances the Therapeutic Efficacy of Immune Checkpoint Blockade Independent of BRCAness

Jianfeng Shen[1], Wei Zhao[2], Zhenlin Ju[2], Lulu Wang[1], Yang Peng[1], Marilyne Labrie[3], Timothy A. Yap[4], Gordon B. Mills[3], and Guang Peng[1]

Abstract

PARP inhibitors (PARPi) have shown remarkable therapeutic efficacy against *BRCA1/2*-mutant cancers through a synthetic lethal interaction. PARPi exert their therapeutic effects mainly through the blockade of ssDNA damage repair, which leads to the accumulation of toxic DNA double-strand breaks specifically in cancer cells with DNA repair deficiency (BCRAness), including those harboring *BRCA1/2* mutations. Here we show that PARPi-mediated modulation of the immune response contributes to their therapeutic effects independently of *BRCA1/2* mutations. PARPi promoted accumulation of cytosolic DNA fragments because of unresolved DNA lesions, which in turn activated the DNA-sensing cGAS–STING pathway and stimulated production of type I IFNs to induce antitumor immunity independent of BRCAness. These effects of PARPi were further enhanced by immune checkpoint blockade. Overall, these results provide a mechanistic rationale for using PARPi as immunomodulatory agents to harness the therapeutic efficacy of immune checkpoint blockade.

Significance: This work uncovers the mechanism behind the clinical efficacy of PARPi in patients with both BRCA-wild-type and BRCA-mutant tumors and provides a rationale for combining PARPi with immunotherapy in patients with cancer.

Introduction

PARP inhibitors (PARPi) are approved for the treatment of patients with ovarian and breast cancers harboring *BRCA1* or *BRCA2* (*BRCA1/2*) mutations (1, 2). The rationale supporting the development of single-agent PARPis in *BRCA1/2*-mutant cancers was based on the concept of synthetic lethality, which predicted antitumor efficacy in tumors with defects in homologous recombination (HR) repair, also known as BRCAness. PARP1 is the most abundant and ubiquitously expressed member of the PARP family and contributes the majority of PARP enzymatic activity and is thus the major target of PARPis (3). In the presence of DNA damage, PARP1 rapidly binds to DNA strand breaks and is essential for the repair of DNA single-strand breaks through base excision repair. In normal cells, recombinogenic DNA substrates generated by PARPis can be functionally resolved by the error-free HR repair pathway. In contrast, in cancer cells with defective HR repair, such as those deficient in BRCA1 or BRCA2, the DNA substrates generated by PARPis cannot be resolved, and therefore the cells are hypersensitive to PARPis (4, 5).

Clinical studies have now also shown patient benefit with PARPis in those with *BRCA1/2* wild-type tumors (6, 7). A recent phase III clinical trial confirmed that patients with platinum-sensitive, recurrent ovarian cancer receiving PARPi treatment as maintenance therapy had significantly longer progression-free survival than those on placebo, regardless of *BRCA1/2* mutation status or HR repair status (7). These clinical observations raise the key question of whether PARPis can exert antitumor effects through mechanisms other than those leading to unresolved genomic lesions in tumors with DNA repair deficiency.

In this study, we show that PARPi treatment induces IFN-mediated antitumor immune responses. PARPis generate cytosolic dsDNA, which activate stimulator of IFN genes (STING) signaling and its associated transcription programs. These critical changes amplify STING signaling, and promote tumor-infiltrating lymphocytes (TIL) and antitumor immunity, which can be further enhanced through immune checkpoint blockade.

Materials and Methods

Cell culture

Cell lines were validated by short tandem repeat (STR) DNA fingerprinting using the AmpF STR Identifier Kit according to the manufacturer's instructions (Applied Biosystems, catalog

[1]Department of Clinical Cancer Prevention, The University of Texas MD Anderson Cancer Center, Houston, Texas. [2]Department of Systems Biology, The University of Texas MD Anderson Cancer Center, Houston, Texas. [3]Department of Cell, Developmental & Cancer Biology, Oregon Health and Science University Knight Cancer Institute, Portland, Oregon. [4]Department of Investigational Cancer Therapeutics, The University of Texas MD Anderson Cancer Center, Houston, Texas.

Note: Supplementary data for this article are available at Cancer Research Online (http://cancerres.aacrjournals.org/).

Corresponding Authors: Guang Peng, University of Texas MD Anderson Cancer Center, 6767 Bertner Ave. S7.8336B, Unit 1013, Houston 77030, TX. Phone: 713-563-6735; Fax: 713-563-5747; E-mail: gpeng@mdanderson.org; and Gordon B. Mills, millsg@ohsu.edu

doi: 10.1158/0008-5472.CAN-18-1003

no. 4322288). The STR profiles were compared with known ATCC fingerprints, with the Cell Line Integrated Molecular Authentication database, version 0.1.200808 (8), and with the MD Anderson fingerprint database. The STR profiles matched known DNA fingerprints or were unique. The colorectal and ovarian cancer cell lines were kindly provided by Dr. Gordon B. Mills' laboratory at The University of Texas MD Anderson Cancer Center (Houston, TX). Cell line authentication was performed in the MD Anderson Characterized Cell Line Core in 2012 and 2013. All media were supplemented with 10% FBS with glutamine, penicillin, and streptomycin. The ID8 mouse ovarian surface epithelial cells were kindly provided by Dr. Vahid Afshar-Kharghan's laboratory at The University of Texas MD Anderson Cancer Center (Houston, TX). The ID8 cells were maintained in DMEM (high-glucose, Cellgro) supplemented with 4% FBS, 100 U/mL penicillin, 100 μg/mL streptomycin, 5 μg/mL insulin, 5 μg/mL transferrin, and 5 ng/mL sodium selenite. Cells were incubated at 37°C in a humidified incubator with 5% CO_2. *Mycoplasma* testing of these cell lines has confirmed negative results.

Antibodies and reagents

Anti-γH2AX (JBW301) antibodies were purchase from Millipore Sigma. Anti-β-actin (A2228), anti-α-Tubulin (T6074), and anti-γ-Tubulin (SAB4503045) antibodies were purchase from Sigma-Aldrich. Anti-STING (D2P2F, catalog no. 13647), anti-cGAS (D1D3G, catalog no. 15102), anti-IRF3 (D6I4C, catalog no. 11904), anti-phospho-IRF3 (Ser396, D6O1M, catalog no. 29047), anti-TBK1 (D1B4, catalog no. 3504), anti-phospho-TBK1 (Ser172, D52C2, catalog no. 5483), anti-CtIP (D76F7, catalog no. 9201), anti-MRE11 (catalog no. 4895), and anti-PD-L1 (13684 and 64988) antibodies were purchased from Cell Signaling Technology. Anti-CD8 (sc-7970), anti-BLM (B-4, sc-365753), anti-EXO1 (SPM394, sc-56387), and other antibodies were purchased from Santa Cruz Biotechnology. BMN673 (S7048, Talazoparib) was purchased from Selleck Chemicals. VivoGlo Luciferin was purchased from Promega. Isotype control IgG and anti-PD-L1 (BE0101, clone 10F.9G2) antibodies were purchased from BioXCell. The ELISA Kits of CCL5 and CXCL10 were purchase from Thermo Fisher Scientific. The multiplexed Immunofluorescence IHC Kit was purchased from PerkinElmer.

RNA interference

Knockdown was achieved by RNA interference using a lentiviral vector–based MISSION shRNA (Sigma-Aldrich). The shRNA sequences were as follows: mouse Sting (NM_028261), TRCN0000346319 (catalog no. 1), AGAGGTCACCGCTCCAAATAT and TRCN0000346266 (catalog no. 2), CAACATTCGATTCCGAGATAT. SMART pool ON-Target plus siRNA for CtIP (L-011376-00), BLM (L-007287-00), EXO1 (L-007287-00), STING (L-024333-02), IRF3 (L-024333-02), TBK1 (L-024333-02), and cGAS (L-015607-02) were purchased from GE Healthcare Dharmacon. Specificity and efficacy of knockdown was evaluated by Western blotting.

Immunoblotting and immunofluorescence

Cells were washed in PBS, and cellular proteins were extracted in 8 mol/L urea lysis buffer plus protease and phosphatase inhibitors (GenDEPOT) for 30 minutes at 4°C. Lysates were cleared by centrifugation, and proteins were separated by gel electrophoresis. Membranes were blocked in PBS 0.1% Tween 20 (PBS-T)/5% (w/v) milk for 1 hour at room temperature. Membranes were then incubated with primary antibodies diluted in PBS-T/5% (w/v) milk at 4°C overnight. Subsequently, membranes were washed with PBS-T and incubated with horseradish peroxidase secondary antibody (1:2,000; Jackson ImmunoResearch) diluted in PBS-T/5% skim milk. Membranes were washed in PBS-T, and bound antibody was detected by Enhanced Chemiluminescence (GE Healthcare Dharmacon). For detection of subcellular localization of IRF3, phospho-IRF3, TBK1, and phospho-TBK1, immunofluorescent staining was performed essentially as described previously (9). After treatment, cells were first fixed in ice-cold methanol for 10 minutes at −20°C, then blocked with 10% goat serum for 30 minutes at room temperature. Primary antibodies (IRF3, 1:200; phospho-IRF3, 1:200; TBK1, 1:200; and phospho-TBK1, 1:100, Cell Signaling Technology) were incubated at 4°C overnight, and Alexa 488- or Alexa 594–conjugated secondary antibodies (1:500, Thermo Fisher Scientific) were incubated for 1 hour at room temperature. Slides were mounted in ProLong antifade mounting medium containing DAPI (Thermo Fisher Scientific) and analyzed under a fluorescence microscope. Nuclear signals of staining were further examined by ImageJ (1.51j8), and the positivity was determined as at least five times greater in nuclear signal compared with the average in control. At least 50 cells per sample were analyzed, and the percentage of cells with positive staining was determined.

PicoGreen staining

PicoGreen staining was performed using Quant-iT Pico-Green dsDNA Reagent and Kits from Thermo Fisher Scientific. For confocal microscopy, PicoGreen was diluted into cell culture medium at the concentration of 3 μL/mL, and the cells were incubated in the presence of PicoGreen at 37 °C for 1 hour. The cells were washed and fixed for confocal microscopy with DAPI counterstaining.

Multiplexed IHC staining

Tumor tissue retrieved from ID8 intraperitoneal injection or CT26 subcutaneous injection was subjected to fixation and paraffin embedding. The sections cut from paraffin blocks were baked at 60°C for 1 hour and deparaffinized and rehydrated with serial passage through changes of xylene and graded alcohol and washed in water. Multiplexed immunofluorescence was performed following the manufacturer's instruction (PerkinElmer). The following antibodies were used for IHC: anti-mouse PD-L1 (D5V3B, Cell Signaling Technology, 1:100), anti-CD8 (H160, Santa Cruz Biotechnology, 1:200), anti-STING (D2P2F, Cell Signaling Technology, 1:100), and anti-phospho-IRF3 (D6O1M, Cell Signaling Technology, 1:100). Stained slides were counterstained with DAPI and coverslipped for review. Positivity was defined as $\geq$5% of staining or the percentage of positive cells per slide was calculated.

Quantitative PCR

Total RNA (1–2 μg) was used in a reverse transcriptase reaction with the High-Capacity RNA-to-cDNA Kit (Thermo Fisher Scientific). The SYBR Green Real-Time PCR Master Mixes Kit (Life Technologies) was used for the thermocycling reaction in an ABI-VIIA7 RealTime PCR Machine (Applied Biosystems). The quantitative PCR analysis was carried out in triplicate with the following primer sets: mouse *Ccl5* (forward: 5′-ATATGGCTCGGACACCACTC-3′; reverse: 5′-TCCTTCGAGTGACAAACACG-3′), mouse *Cxcl10* (forward: 5′-CCCACGTGTTGAGATCATTG-3′;

reverse: 5′-GTGTGTGCGTGGCTTCACT-3′), mouse *Gapdh* (forward: 5′- ACCCAGAAGACTGTGGATGG-3′; reverse: 5′- ACACATTGGGGGTAGGAAC-3′), human *CCL5* (forward: 5′-TGCCCACATCAAGGAGTATTT-3′; reverse: 5′-CTTTCGGGTGACAAAGACG-3′), human *CXCL10* (forward: 5′-GGCCATCAAGAATTTACTGAAAGCA-3′; reverse: 5′- TCTGTGTGGTCCATCCTTGGAA-3′), and human β-Actin (forward: 5′-GAGCACAGAGCCTCGCCTTT-3′; reverse: 5′-TCATCATCCATGGTGAGCTG-3′).

ELISA

The cell culture supernatant or ascites from ID8 model were collected and processed according to the manufacturer's instructions. The CXCL10 and CCL5 levels were determined using ELISA Kits from R&D/Thermo Fisher Scientific following the standard procedures.

In vivo mouse models

All studies were supervised and approved by the MD Anderson Institutional Animal Care and Use Committee (IACUC). Female mice were used as models to study ovarian cancer. When used in a power calculation, our sample size predetermination experiments indicated that 5 mice per group could identify the expected effects with 90% power.

Ovarian cancer syngeneic model

Luciferase-labeled ID8 ovarian cancer cells (5×10^6) were injected into the peritoneal cavity of C57BL/6 mice per group (6–8 weeks old, CRL/NCI). STING knockout mice (*Tmem173 gt/J*) were purchased from The Jackson laboratory (catalog no. 017537). The mice were allowed to recover and were monitored closely for the next 24 hours. Tumor progression was monitored once per week by Xenogen IVIS spectrum *in vivo* bioluminescence imaging system. Tumor volume was determined on the basis of total flux (photons/second). Tumor-bearing mice were treated intraperitoneally with isotype control IgG or anti-PD-L1 antibody (200 μg/mouse, B7-H1, clone 10F.9G2, BioXCell) every 3 days. BMN673 was administered by daily oral gavage with a dose of 0.33 mg/kg. Mice reaching an endpoint requiring euthanasia by IACUC guidelines or weighing more than 35 grams as a result of tumor growth and/or ascites were euthanized.

Colorectal cancer syngeneic model

Murine CT26 colorectal cancer cells (2×10^5) were subcutaneously injected into the left flank of BALB/c mice (6–8 weeks old, CRL/NCI) as described previously. Mice were allowed to recover and monitored closely for the next 24 hours. Tumor size was measured every 3 days and tumor volume was determined on the basis of the calculation (width × width × length)/2. Tumor-bearing mice were treated intraperitoneally with isotype control IgG or anti-PD-L1 antibody (200 μg/mouse, B7-H1, clone 10F.9G2, BioXCell) every 3 days. BMN673 was administered by daily oral gavage with a dose of 0.33 mg/kg. Mice reaching an endpoint requiring euthanasia by IACUC guidelines or exceeding tumor burden limits were euthanized.

Colorectal cancer nude mouse model

Nude mouse experiments were conducted as described previously. Briefly, murine colorectal cancer cells CT26 (2×10^5) were subcutaneously injected into the left flank of athymic nude mice (6–8 weeks old, CRL/NCI). Mice were allowed to recover and monitored closely for the next 24 hours. Tumor size was measured every 3 days and the tumor volume was determined on the basis of the calculation (width × width × length)/2. Tumor-bearing mice were treated intraperitoneally with isotype control IgG or anti-PD-L1 antibody (200 μg/mouse, B7-H1, clone 10F.9G2, BioXCell) every 3 days. BMN673 was administered by daily oral gavage with a dose of 0.33 mg/kg. Mice reaching an endpoint requiring euthanasia by IACUC guidelines or exceeding tumor burden limits were euthanized.

Ovarian cancer nude mouse model

Luciferase-labeled ID8 cells (5×10^6) were injected into peritoneal cavity of athymic nude mice (6–8 weeks old, CRL/NCI). Mice were allowed to recover and monitored closely for the next 24 hours. Tumor progression was monitored once a week by Xenogen IVIS spectrum *in vivo* bioluminescence imaging system. Tumor volume was determined on the basis of total flux (photons/second). Tumor-bearing mice were treated intraperitoneally with isotype control IgG or anti-PD-L1 antibody (200 μg/mouse, B7-H1, clone 10F.9G2, BioXCell) every 3 days. BMN673 were administered by daily oral gavage with a dose of 0.33 mg/kg. Mice reaching an endpoint requiring euthanasia by IACUC guidelines or weighing more than 35 grams as a result of tumor growth and/or ascites were euthanized.

Statistical analysis

All statistical analyses were done in GraphPad Prism 7 software. Overall survival of various treatment groups was analyzed using the Cox regression model. Otherwise, unpaired *t* tests were used to generate two-tailed *P* values.

Results

PARPi induces an accumulation of cytosolic DNA and activates STING signaling pathway

PARPi treatment markedly induced DNA double-strand breaks (DSB) as detected by increased γH2AX levels, and thus caused cell-cycle arrest in S phase (Supplementary Fig. S1A and S1B). The cytosolic DNA sensor cyclic GMP-AMP synthase (cGAS) is the most potent activator of the STING signaling pathway (10). After the recognition of cytosolic DNA, cGAS activates STING via generation of 2′-5′ cyclic GMP-AMP (cGAMP). STING, in turn, induces phosphorylation and nuclear translocation of IFN transcriptional regulatory factors TANK-binding kinase 1 (TBK1) and IFN regulatory factor 3 (IRF3; refs. 11, 12). We thus examined whether PARPi induces accumulation of cytosolic DNA that could activate the cGAS–STING–TBK1–IRF3 axis in ovarian cancer cell lines HOC1 (*BRCA1/2* WT), UPN251 (*BRCA1* deleterious and restoration mutations, and functional wild-type; ref. 13), and HeLa (*BRCA1/2* WT).

As shown in Fig. 1A, BMN673 caused a significant accumulation of cytosolic dsDNA in multiple cell lines. Moreover, phosphorylation of IRF3 and TBK1, two key components along the STING pathway, was markedly elevated by BMN673 treatment in a time-dependent manner (Fig. 1B). PARPi also remarkably induced the translocation of phospho-IRF3, phospho-TBK1 (Fig. 1B), as well as total IRF3 and total TBK1 from the cytoplasm to the nucleus (Supplementary Fig. S2A), which indicated functional activation of STING signaling. We then examined mRNA expression of *CCL5* and *CXCL10*, two major

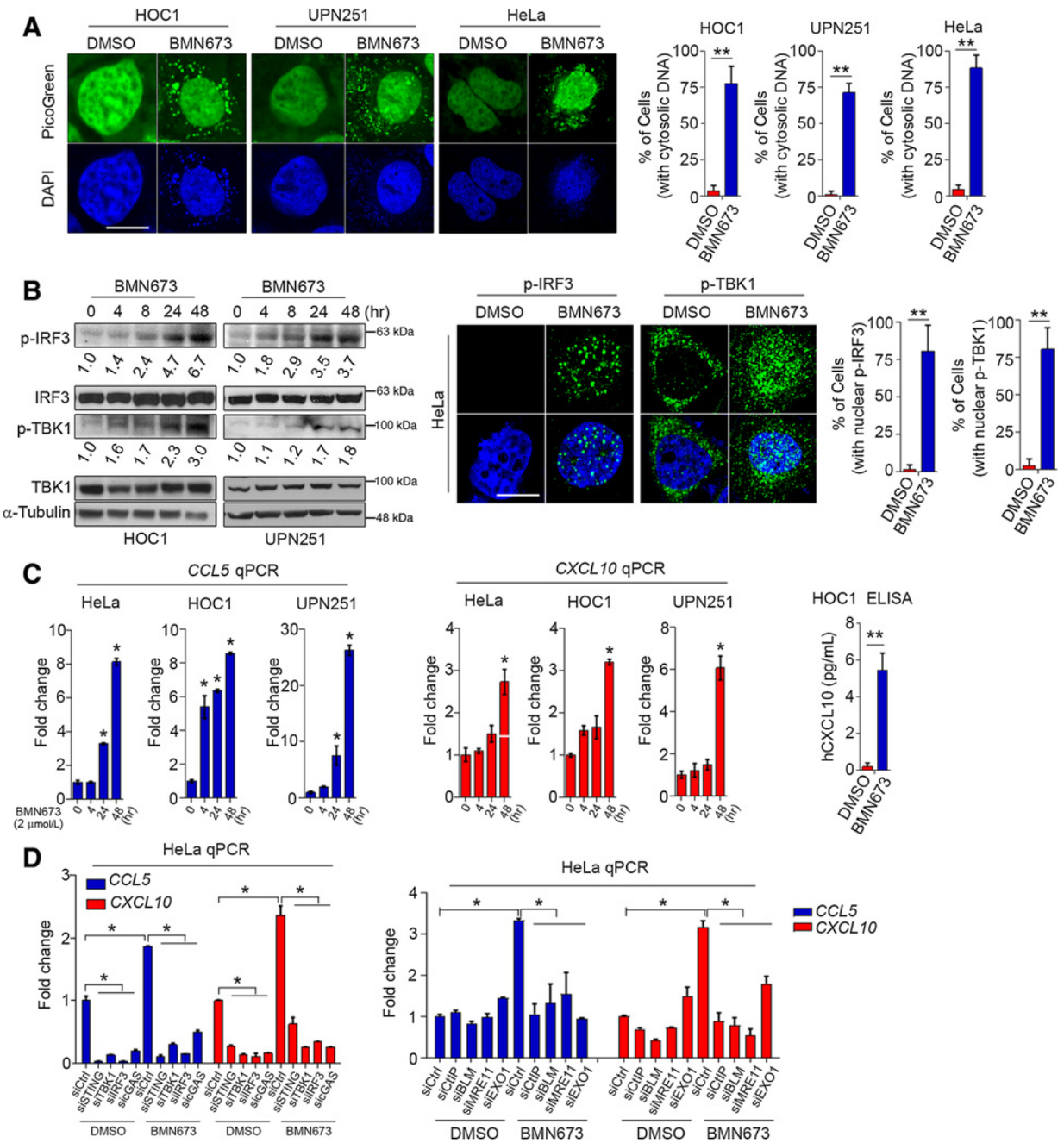

Figure 1.

PARPi induces accumulation of cytosolic DNA and activates the STING signaling pathway. **A,** Representative images and quantitative analysis of PicoGreen staining in cells treated with DMSO or BMN673 (2 μmol/L) for 48 hours. DAPI (blue) was used to visualize the nuclei. Data represent mean ± SEM of three independent experiments. **B,** Western blots (left) and immunofluorescent images (right) of phosphorylated IRF3 (p-IRF3) and phosphorylated TBK1 (p-TBK1) in cells treated with BMN673 (2 μmol/L). The numbers represent the folds change of p-IRF3 and p-TBK1 from three independent experiments. For immunofluorescence staining, HeLa cells were treated with DMSO or BMN673 (2 μmol/L) for 48 hours. Data represent mean ± SEM of three independent experiments. **C,** qPCR and ELISA evaluation of *CCL5* and *CXCL10* expression in cells under DMSO or BMN673 treatment. For ELISA analysis, HOC1 cells were treated with DMSO or BMN673 treatment for 48 hours. Data represent mean ± SEM of three independent experiments. **D,** qPCR evaluation of *CCL5* and *CXCL10* levels in HeLa cells with depletion of STING (siSTING), TBK1 (siTBK1), IRF3 (siIRF3), cGAS (sicGAS), CtIP (siCtIP), BLM (siBLM), MRE11 (siMRE11), or EXO1 (siEXO1). Cells were treated with DMSO or BMN673 (2 μmol/L) for 48 hours. Data represent mean ± SEM of three independent experiments. Scale bar, 10 μm. *, $P < 0.05$; **, $P < 0.01$.

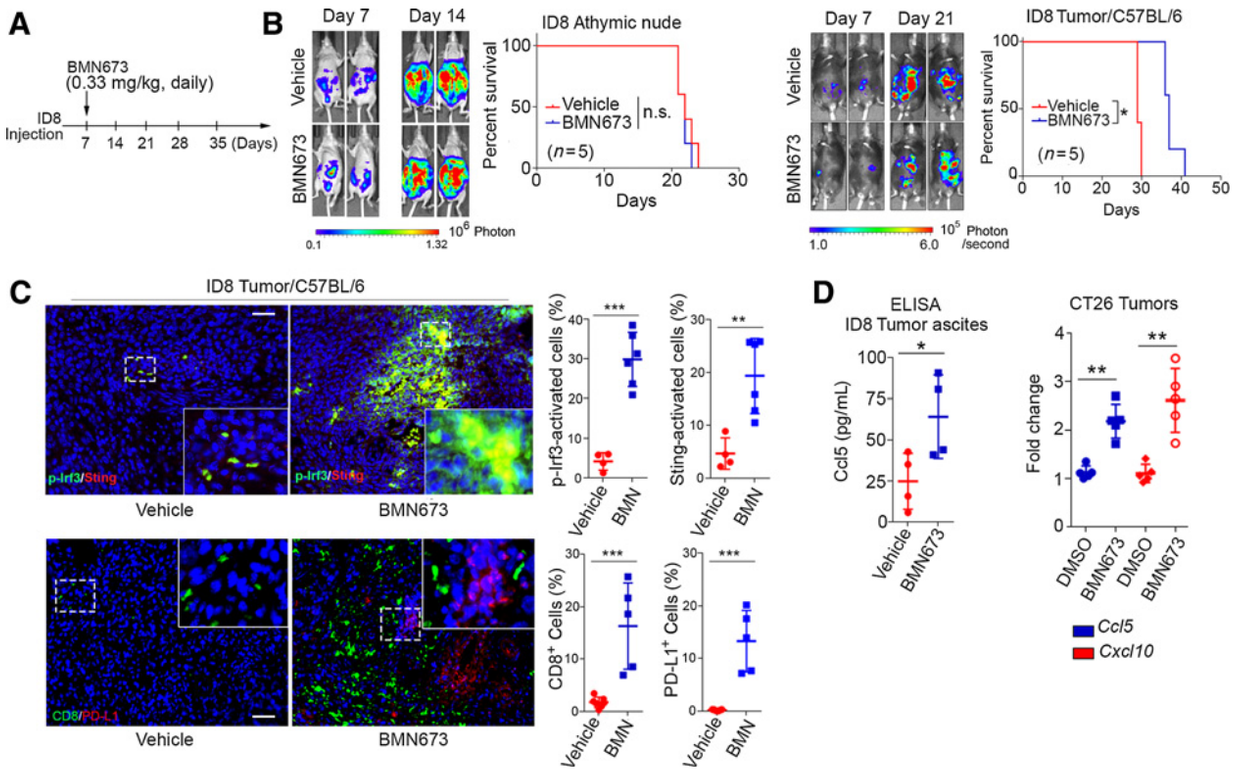

Figure 2.

PARPi activates STING signaling and immune checkpoint *in vivo*. **A,** Schematic of PARPi treatment in nude and syngeneic mice bearing intraperitoneal ID8 tumors. Mice were treated with BMN673 (0.33 mg/kg) daily by oral administration 7 days after ID8 inoculation until euthanization ($n = 5$). **B,** Representative bioluminescence images of intraperitoneal tumors in immune-deficient (left) and immune-proficient (right) mice on day 7 and day 21 of ID8 cell inoculation and survival curves. **C,** Representative images and quantitative analysis of phosphorylated Irf3 (p-Irf3), Sting, CD8, and PD-L1 in ID8 tumors 30 days after inoculation. DAPI (blue) was used to visualize the nuclei. **D,** ELISA evaluation of Ccl5 levels in ascites from C57BL/6 mice when euthanization was performed (left) and qPCR evaluation of *Ccl5* and *Cxcl10* levels in CT26 tumors from BALB/c mice 22 days after tumor cell inoculation (right). Dashed square, area for magnification. Scale bar, 50 μm. *, $P < 0.05$; **, $P < 0.01$; ***, $P < 0.001$; n.s., not significant.

target genes downstream of STING activation that are involved in T-cell chemotaxis (14). We found a time-dependent increase in *CCL5* and *CXCL10* mRNA levels after PARPi treatment (Fig. 1C). Consistent with these changes in mRNA levels, PARPi substantially increased the production of CXCL10 as detected by ELISA (Fig. 1C). We further found that upregulation of *CCL5* and *CXCL10* was significantly reduced in response to PARPi treatment in cells with STING, TBK1, IRF3, or cGAS knockdown (Fig. 1D; Supplementary Fig. S2B–S2D; and Supplementary Fig. S3A). Together, these results demonstrate that PARPi induces accumulation of cytosolic dsDNA and activation of cGAS–STING–TBK1–IRF3 signaling to promote chemokine expression.

Several key factors containing and/or regulating nuclease activity, including MRE11, CtIP, BLM, and EXO1, are recruited to DSBs, which can produce DNA fragments during HR repair and maintenance of replication fork stability (15). We reasoned that trapping of PARP1 by PARPi forms a barrier against DSB end resection and HR repair, which may lead to generation of dsDNA through degradation of unrepaired reversed replication forks. Indeed, we demonstrated that knockdown of these resection factors by siRNAs markedly reduced mRNA expression of *CCL5* and *CXCL10* (Fig. 1D; Supplementary Fig. S3B), suggesting a key role for the requirement of these factors in generating PARPi-induced immune responses.

PARPi activates STING signaling and immune checkpoint *in vivo*

We next investigated the *in vivo* effects of PARPi-induced immune responses, using syngeneic immunocompetent mouse models of ovarian cancer (ID8) and colon cancer (CT26). CT26 and ID8 cells have no known mutations in genes involved in the HR repair pathway, including *BRCA1/2* mutations. As expected, PARPi treatment exhibited no therapeutic effects in immunodeficient mice bearing ID8 tumors (Fig. 2A and B). In contrast, PARPi can reduce tumor growth and prolong survival in the ID8 syngeneic model (Fig. 2B). These data indicated that an intact T-cell–mediated immune response is required for PARPi efficacy in the ID8 model.

It has been reported that expression levels of *CCL5* and *CXCL10* positively correlate with infiltrating $CD8^+$ cytotoxic lymphocytes in various cancers (16). We thus conducted IHC analysis of STING activation and immune response. In syngeneic ID8 and CT26 models, PARPi significantly upregulated the levels of Irf3 phosphorylation as well as Sting expression, indicating robust activation of the Sting signaling pathway

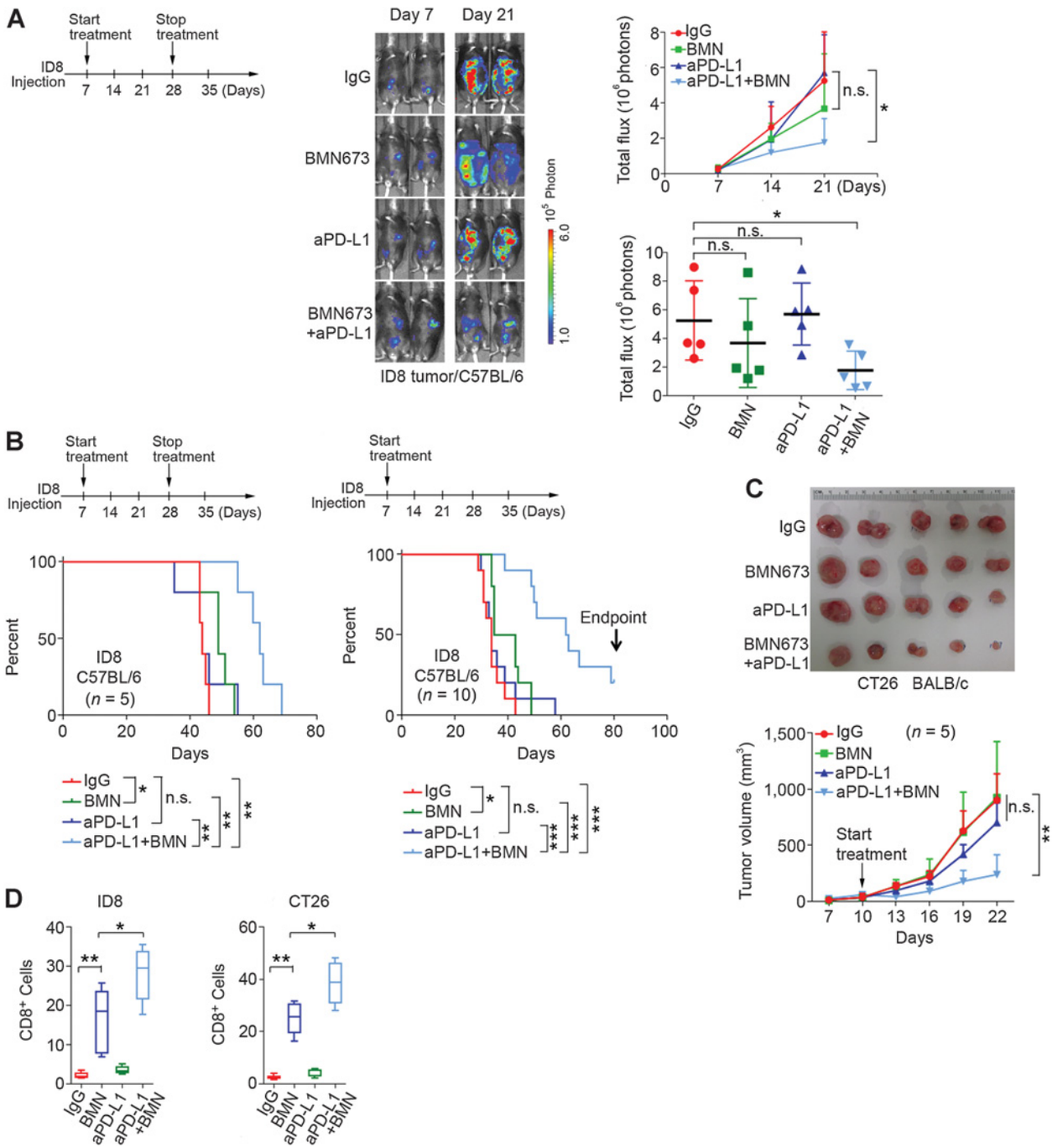

Figure 3.

Immune checkpoint blockade targeting PD-1/PD-L1 pathway potentiates therapeutic efficacy of PARPi in syngenic mouse models. **A,** Combination treatment in C57BL6 mice bearing ID8 tumors. Left, schematic of treatment. Intraperitoneal injections of isotype control IgG (200 μg/mouse) and anti-PD-L1 antibody (aPD-L1, 200 μg/mouse) started at day 7 and stopped at day 28 after ID8 cell inoculation. BMN673 (0.33 mg/kg) was orally administered daily. Middle, representative bioluminescence images of ID8 tumors after 7 and 21 days of inoculation. Right, statistical analysis of bioluminescence changes over time (mean ± SEM) or at the endpoint (day 21, each dot represents one mouse; $n = 5$). **B,** Survival curves of mice with temporary (left, started on day 7 after ID8 inoculation and stopped on day 28; $n = 5$) or continuous treatment (right, started on day 7 after inoculation and continued until the mice were euthanized; $n = 10$). **C,** Representative images and tumor volume measurements of CT26 tumors in BALB/c mice with continuous treatment ($n = 5$). **D,** Percentage of $CD8^+$ cells in ID8 or CT26 tumors after treatments. *, $P < 0.05$; **, $P < 0.01$; ***, $P < 0.001$; n.s., not significant.

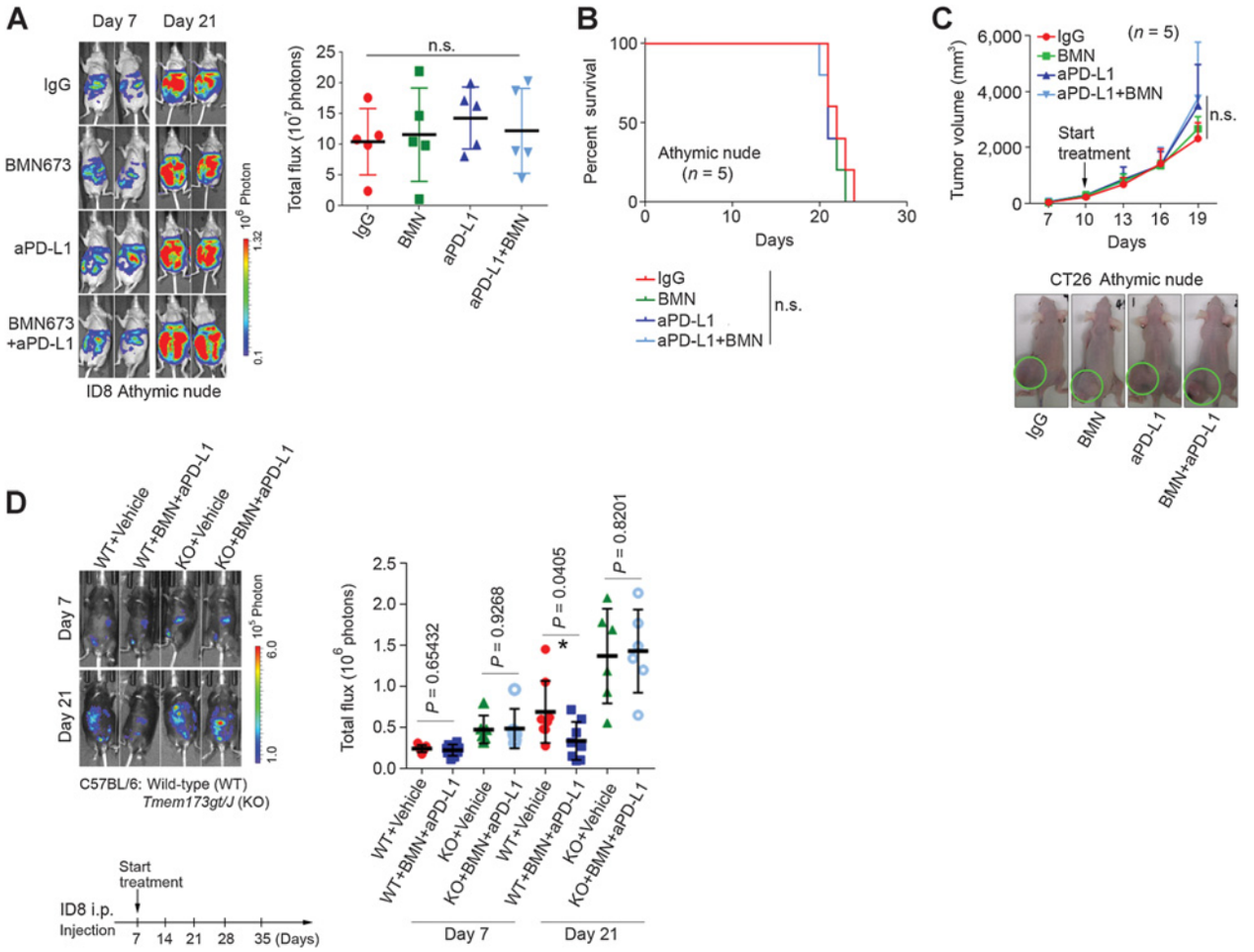

Figure 4.

An intact immune system is required for the therapeutic benefits of combining PARPi with anti-PD-L1. **A,** Representative images and statistical analysis of endpoint bioluminescence in athymic nude mice bearing ID8 intraperitoneal tumors. Data represent mean ± SEM, ($n = 5$). Intraperitoneal injection of isotype control IgG (200 μg/mouse) and anti-PD-L1 (aPD-L1, 200 μg/mouse) was started at day 7 and continued until mice were euthanized. BMN673 (0.33 mg/kg) was orally administered daily. **B,** Survival curves of athymic nude mice with ID8 intraperitoneal tumors. Treatment was started on day 7 and continued until mice were euthanized. **C,** Representative images and tumor volume measurements of CT26 tumors in athymic nude mice with the indicated treatments ($n = 5$). n.s., not significant. **D,** Representative images and statistical analysis of bioluminescence in wild-type (WT) or STING knockout (KO, *Tmem173 gt/J*) mice bearing ID8 intraperitoneal tumors. Intraperitoneal injection of vehicle (isotype control IgG, 200 μg/mouse) and anti-PD-L1 (aPD-L1, 200 μg/mouse) was started at day 7 and continued. BMN673 (0.33 mg/kg) was orally administered daily.

in vivo (Fig. 2C; Supplementary Fig. S4A). Consistent with this finding, remarkably higher percentages of $CD8^+$ T cells and $PD\text{-}L1^+$ cells were found in PARPi-treated tumors (Fig. 2C; Supplementary Fig. S4B). Furthermore, as shown in Fig. 2D, PARPi treatment induced expression of Ccl5 and Cxcl10, which was consistent with *in vitro* studies (Fig. 1). Together, these data showed that PARPi treatment induces an immunogenic response through the activation of the STING pathway and enhancement of type I IFN response and TILs *in vivo*. However, activation of the PD-1/PD-L1 immune checkpoint pathway may counterbalance the impact of active TILs and block elimination of tumor cells despite the immunogenic microenvironment induced by PARPi. These results raised the possibility that the combination of immune checkpoint blockade and PARPi would synergistically limit tumor growth and prolong survival.

Immune checkpoint blockade targeting PD-1/PD-L1 pathway potentiates therapeutic efficacy of PARPi in syngeneic mouse models

To test this possibility, we first treated mice with ID8 for 3 weeks and then stopped treatment. Consistent with relatively poor immunogenicity and low TILs in ID8 tumors (17), ID8 tumors did not significantly respond to anti-PD-L1 therapy or BMN673 alone after 3 weeks of treatment (Fig. 3A). Only the combination significantly reduced tumor growth while no significant changes in mouse weight were observed (Fig. 3A; Supplementary Fig. S4C). In the third week of treatment, mice developed ascites, which interfered with further luciferase measurements, but the study was continued to measure survival. As shown in Fig. 3B, only the combination treatment significantly prolonged survival. Continuous treatment with the combination of BMN673 and

anti-PD-L1 produced a remarkably better outcome than 3-week treatment (Fig. 3B), suggesting a potential curative effect from this continuous regimen.

We next used CT26 mouse colon tumor cells as an independent syngeneic model to validate the efficacy of combination therapy. Because CT26 tumors grew aggressively, mice were treated for 12 days before the tumor size reached the maximum volume allowed by the animal protocol. The combination therapy significantly reduced CT26 tumor burden compared with IgG control (Fig. 3C). Although BMN673 increased the percentage of tumor-infiltrating $CD8^+$ cells (Supplementary Fig. S4B), these tumors were not sensitive to BMN673 alone. The combination of BMN673 and anti-PD-L1 treatment results in the most significant increase of $CD8^+$ cells in both ID8 and CT26 models (Fig. 3D).

The therapeutic effects of combining PARPi and anti-PD-L1 depend on an intact immune system

Interestingly, none of the treatments examined, BMN673 monotherapy, anti-PD-L1 monotherapy, and the combination of BMN673 and anti-PD-L1, inhibited tumor growth or improved survival in immunocompromised nude mouse models bearing ID8 or CT26 tumors (Fig. 4A–C). These results strongly supported the notion that an intact immune system is a prerequisite to achieve the benefits of combination therapy. More importantly, in a STING-knockout mouse model, we found that lack of STING abolished antitumor effects of PARPi and anti-PD-L1 treatment on ID8 tumors, demonstrating that STING signaling is genetically required for therapeutic effects of PARPi and anti-PD-L1 treatment (Fig. 4D).

Discussion

Here we show PARPi leads to an accumulation of cytosolic dsDNA and thereby activates the cGAS–STING–TBK1–IRF3 innate immune pathway, which induces type I IFN and its related immune responses (Supplementary Fig. S4D). Furthermore, PARPi treatment enhances tumor susceptibility to immune checkpoint blockade. Importantly, these responses were observed regardless of the *BRCA1/2* mutation status of the cell lines assessed both *in vitro* and *in vivo*.

Recent studies have shown that micronuclei resulting from missegregation of DNA during cell division can be recognized by the cytosolic DNA sensor cGAS and activate the STING innate immune pathway (18). Our data uncovered that DNA damage induced by PARPi generates cytosolic DNA, primarily dsDNA. PARPis induces stalled or collapsed replication forks. dsDNA generated by PARPi may be related to DNA replication fork degradation/reversion or the restart of replication. Our study thus proposes a novel molecular mechanism underlying PARPi therapeutic effects, which is independent of its conventional cytotoxic effects resulting from unresolved DNA damage in DNA repair–deficient cancer cells.

The antitumor activity of PARPi has been observed in patients regardless of *BRCA1/2* mutation status or the presence of HR defects (7). Our results also support this notion because the immunogenic responses induced by PARPi are not dependent on DNA repair deficiency. However, treatment with a single agent of PARPi is not sufficient to exert durable therapeutic effects. This phenomenon may be explained by the overall impact of PARPi on tumor microenvironment. CCL5 and CXCL10 are chemokines that associate with recruitment of TILs and their production is relevant to trigger proper antitumor immune responses (19, 20). However, an increasing number of studies have demonstrated that CCL5 may favor tumor growth through myeloid cell recruitment (21, 22). Of note, myeloid cells are essential to activate immune checkpoint PD-1/PD-L1 axis thereby are required for the establishment of an immunosuppressive tumor microenvironment in multiple cancer types (23–25). Significant increase in number of PD-$L1^+$ cells in ID8 and CT26 tumors indicate that PARPi may recruit myeloid cells into tumor sites and, therefore, counterbalance the therapeutic efficacy. It is possible that the benefits of combining PARPi with anti-PD-L1 may be further strengthened by inhibiting the immunosuppressive myeloid cells.

Disclosure of Potential Conflicts of Interest

T.A. Yap reports receiving other commercial research support from AstraZeneca, Bayer, Pfizer, Tesaro, Jounce, Eli Lilly, Seattle Genetics, Kyowa, Constellation, and Vertex Pharmceuticals, has received speakers bureau honoraria from AstraZeneca, Merck, Pfizer, and Tesaro, and is a consultant/advisory board member for Aduro, Almac, Ignyta, Jansen, Merck, Pfizer, Roche, Seattle Genetics, Vertex Pharmaceuticals, AstraZeneca, Atrin, Bayer, Bristol-Meyers Squibb, Calithera, Clovis, Cybrexa, and EMD Serono. G.B. Mills reports receiving commercial research grant from Ovarian Cancer Research Foundation, Adelson Medical Research Foundation, NanoString Technologies, Susan G. Komen Breast Cancer Foundation, Breast Cancer Research Foundation, Karus Therapeutics Ltd., AstraZeneca, Ionis, Pfizer Pharmaceuticals (including the current research), ImmunoMet, and Tesaro, Inc, other commercial research support from Prospect Creek Foundation and Takeda/Millienium Pharmaceuticals, has ownership interest (including stock, patents, etc.) in Catena Pharmaceuticals, ImmunoMet, SignalChem, Spindletop Ventures, and Tarveda, and is a consultant/advisory board member for AstraZeneca, Catena Pharmaceuticals, Tesaro, Critical Outcome Technologies, ImmunoMET, Ionis, Signalchem Lifesciences, Symphogen, Takeda/Millenium Pharmaceuticals, Tarveda, and Nuevolution. G. Peng received sponsored research funding from Pfizer (including the current research). No potential conflicts of interest were disclosed by the other authors.

Authors' Contributions

Conception and design: J. Shen, T.A. Yap, G.B. Mills, G. Peng
Development of methodology: J. Shen, G. Peng
Acquisition of data (provided animals, acquired and managed patients, provided facilities, etc.): J. Shen, L. Wang, Y. Peng, M. Labrie, G. Peng
Analysis and interpretation of data (e.-g., statistical analysis, biostatistics, computational analysis): J. Shen, W. Zhao, Z. Ju, L. Wang, G.B. Mills, G. Peng
Writing, review, and/or revision of the manuscript: J. Shen, W. Zhao, T.A. Yap, G.B. Mills, G. Peng
Administrative, technical, or material support (i.e., reporting or organizing data, constructing databases): J. Shen, G. Peng
Study supervision: G. Peng

Acknowledgments

This research was supported by NCI Cancer Center Support Grant CA016672 to The University of Texas MD Anderson Cancer Center, Department of Defense grant OC140431and NIH R01 grant CA181663 to G. Peng, Cancer Prevention and Research Institute of Texas grant RP160242 to G. Peng and X. Shen, and the Adelson Medical Research Foundation and Cancer Prevention and Research Institute of Texas grant RP 170640 to G. Mills.

Received April 3, 2018; revised August 13, 2018; accepted November 20, 2018; published first November 27, 2018.

References

1. Fong PC, Boss DS, Yap TA, Tutt A, Wu P, Mergui-Roelvink M, et al. Inhibition of poly(ADP-ribose) polymerase in tumors from BRCA mutation carriers. N Engl J Med 2009;361:123–34.
2. Ledermann J, Harter P, Gourley C, Friedlander M, Vergote I, Rustin G, et al. Olaparib maintenance therapy in platinum-sensitive relapsed ovarian cancer. N Engl J Med 2012;366:1382–92.
3. Ray Chaudhuri A, Nussenzweig A. The multifaceted roles of PARP1 in DNA repair and chromatin remodelling. Nat Rev Mol Cell Biol 2017;18:610–21.
4. Bryant HE, Schultz N, Thomas HD, Parker KM, Flower D, Lopez E, et al. Specific killing of BRCA2-deficient tumours with inhibitors of poly(ADP-ribose) polymerase. Nature 2005;434:913–7.
5. Farmer H, McCabe N, Lord CJ, Tutt AN, Johnson DA, Richardson TB, et al. Targeting the DNA repair defect in BRCA mutant cells as a therapeutic strategy. Nature 2005;434:917–21.
6. Gelmon KA, Tischkowitz M, Mackay H, Swenerton K, Robidoux A, Tonkin K, et al. Olaparib in patients with recurrent high-grade serous or poorly differentiated ovarian carcinoma or triple-negative breast cancer: a phase 2, multicentre, open-label, non-randomised study. Lancet Oncol 2011;12:852–61.
7. Mirza MR, Monk BJ, Herrstedt J, Oza AM, Mahner S, Redondo A, et al. Niraparib maintenance therapy in platinum-sensitive, recurrent ovarian cancer. N Engl J Med 2016;375:2154–64.
8. Romano P, Manniello A, Aresu O, Armento M, Cesaro M, Parodi B. Cell Line Data Base: structure and recent improvements towards molecular authentication of human cell lines. Nucleic Acids Res 2009;37:D925–32. doi: 10.1093/nar/gkn730.
9. Pourcelot M, Zemirli N, Silva Da Costa L, Loyant R, Garcin D, Vitour D, et al. The Golgi apparatus acts as a platform for TBK1 activation after viral RNA sensing. BMC Biol 2016;14:69.
10. Ablasser A, Goldeck M, Cavlar T, Deimling T, Witte G, Rohl I, et al. cGAS produces a 2'-5'-linked cyclic dinucleotide second messenger that activates STING. Nature 2013;498:380–4.
11. Corrales L, McWhirter SM, Dubensky TW Jr, Gajewski TF. The host STING pathway at the interface of cancer and immunity. J Clin Invest 2016;126:2404–11.
12. Ma Z, Damania B. The cGAS-STING defense pathway and its counteraction by viruses. Cell Host Microbe 2016;19:150–8.
13. Stordal B, Timms K, Farrelly A, Gallagher D, Busschots S, Renaud M, et al. BRCA1/2 mutation analysis in 41 ovarian cell lines reveals only one functionally deleterious BRCA1 mutation. Mol Oncol 2013;7:567–79.
14. Parkes EE, Walker SM, Taggart LE, McCabe N, Knight LA, Wilkinson R, et al. Activation of STING-dependent innate immune signaling by S-phase-specific DNA damage in breast cancer. J Natl Cancer Inst 2017;109:djw199.
15. Longhese MP, Bonetti D, Manfrini N, Clerici M. Mechanisms and regulation of DNA end resection. EMBO J 2010;29:2864–74.
16. Muthuswamy R, Berk E, Junecko BF, Zeh HJ, Zureikat AH, Normolle D, et al. NF-kappaB hyperactivation in tumor tissues allows tumor-selective reprogramming of the chemokine microenvironment to enhance the recruitment of cytolytic T effector cells. Cancer Res 2012;72:3735–43.
17. Buckanovich RJ, Facciabene A, Kim S, Benencia F, Sasaroli D, Balint K, et al. Endothelin B receptor mediates the endothelial barrier to T cell homing to tumors and disables immune therapy. Nat Med 2008;14:28–36.
18. Harding SM, Benci JL, Irianto J, Discher DE, Minn AJ, Greenberg RA. Mitotic progression following DNA damage enables pattern recognition within micronuclei. Nature 2017;548:466–70.
19. Hanahan D, Coussens LM. Accessories to the crime: functions of cells recruited to the tumor microenvironment. Cancer Cell 2012;21:309–22.
20. Tokunaga R, Zhang W, Naseem M, Puccini A, Berger MD, Soni S, et al. CXCL9, CXCL10, CXCL11/CXCR3 axis for immune activation - a target for novel cancer therapy. Cancer Treat Rev 2018;63:40–7.
21. Schlecker E, Stojanovic A, Eisen C, Quack C, Falk CS, Umansky V, et al. Tumor-infiltrating monocytic myeloid-derived suppressor cells mediate CCR5-dependent recruitment of regulatory T cells favoring tumor growth. J Immunol 2012;189:5602–11.
22. Dutta P, Nahrendorf M. Regulation and consequences of monocytosis. Immunol Rev 2014;262:167–78.
23. Zhang Y, Velez-Delgado A, Mathew E, Li D, Mendez FM, Flannagan K, et al. Myeloid cells are required for PD-1/PD-L1 checkpoint activation and the establishment of an immunosuppressive environment in pancreatic cancer. Gut 2017;66:124–36.
24. Antonios JP, Soto H, Everson RG, Moughon D, Orpilla JR, Shin NP, et al. Immunosuppressive tumor-infiltrating myeloid cells mediate adaptive immune resistance via a PD-1/PD-L1 mechanism in glioblastoma. Neuro Oncol 2017;19:796–807.
25. Elliott LA, Doherty GA, Sheahan K, Ryan EJ. Human tumor-infiltrating myeloid cells: phenotypic and functional diversity. Front Immunol 2017;8:86.